The EMBO Journal (2008) 27, 253–264 | © 2008 European Molecular Biology Organization | All Rights Reserved 0261-4189/08
www.embojournal.org

THE
EMBO
JOURNAL

Molecular basis of the C-terminal tail-to-tail assembly of the sarcomeric filament protein myomesin

Nikos Pinotsis[1], Stephan Lange[2], Jean-Claude Perriard[3], Dmitri I Svergun[1,4] and Matthias Wilmanns[1,*]

[1]EMBL-Hamburg c/o DESY, Hamburg, Germany, [2]School of Medicine, University of California, San Diego, La Jolla, CA, USA, [3]Institute of Cell Biology, ETH Zurich-Hönggerberg, Zurich, Switzerland and [4]Institute of Crystallography, Russian Academy of Sciences, Moscow, Russia

Sarcomeric filament proteins display extraordinary properties in terms of protein length and mechanical elasticity, requiring specific anchoring and assembly mechanisms. To establish the molecular basis of terminal filament assembly, we have selected the sarcomeric M-band protein myomesin as a prototypic filament model. The crystal structure of the myomesin C-terminus, comprising a tandem array of two immunoglobulin (Ig) domains My12 and My13, reveals a dimeric end-to-end filament of 14.3 nm length. Although the two domains share the same fold, an unexpected rearrangement of one β-strand reveals how they are evolved into unrelated functions, terminal filament assembly (My13) and filament propagation (My12). The two domains are connected by a six-turn α-helix, of which two turns are void of any interactions with other protein parts. Thus, the overall structure of the assembled myomesin C-terminus resembles a three-body beads-on-the-string model with potentially elastic properties. We predict that the found My12-helix-My13 domain topology may provide a structural template for the filament architecture of the entire C-terminal Ig domain array My9–My13 of myomesin.

The EMBO Journal (2008) **27,** 253–264. doi:10.1038/sj.emboj.7601944; Published online 6 December 2007
Subject Categories: cell & tissue architecture; structural biology
Keywords: filament; M band; muscle sarcomere; myomesin; protein assembly

Introduction

The sarcomeric units of skeletal and cardiac muscles contain one of the most complex multiprotein assemblies characterized to date. Many of these protein components, which function either as filaments or filament bridges, are composed of long arrays of immunoglobulin (Ig)-like and fibronectin type III (Fn) domains (Kenny *et al*, 1999; Li *et al*, 2002; Tskhovrebova and Trinick, 2003; Williams *et al*, 2003). As many of these proteins actively contribute to the force generating apparatus of muscle cells, they need to have elastic properties that support reversible conformational changes in response to these forces. As a prerequisite, these filament systems need to be tightly assembled and anchored within stable subcellular structures, such as the Z-disk and M-band of the sarcomeric unit. These processes frequently take place at one or both termini of the respective sequences.

The giant muscle protein titin is a prototype protein for investigations aimed at unraveling the underlying molecular mechanisms for filament anchoring, assembly and elasticity (Watanabe *et al*, 2002; Lange *et al*, 2006; Sotomayor and Schulten, 2007). The molecular basis of the N-terminal telethonin-mediated assembly of titin in the Z-disk has been recently elucidated (Zou *et al*, 2006). However, it is unlikely that this unique arrangement could serve as a model for the terminal assembly of other sarcomeric filaments. Biochemical data indicated that the C-terminal M-band portion of titin is cross-linked with myosin and myomesin filaments by yet unknown molecular mechanisms (Obermann *et al*, 1996). The potential importance of these interactions has been underlined by recent studies on targeting the C-terminal M-band region of titin in embryonic stem cells or animals, revealing extensive defects in myofibrillogenesis and in the maturation and maintenance of intact sarcomeres (Weinert *et al*, 2006).

To unravel the general molecular principles in the assembly of long sarcomeric proteins, we have selected the M-band protein myomesin as a molecular model. Myomesin and M-protein resemble the giant muscle protein titin in terms of modular domain composition and structure (Vinkemeier *et al*, 1993; Labeit *et al*, 1997). The C-terminal regions of both proteins are composed of five modular Ig-like domains interspersed at regular sequence intervals. Whereas myomesin is generally found in all vertebrate striated-muscle types, M-protein is specifically expressed during late embryonic heart development and appears to be absent in adult slow-twitch muscles, indicating that these two homologous proteins exhibit different functions (Obermann *et al*, 1996). An early model of the M-band displayed myomesin as a filament bridge connecting myosin with titin (Obermann *et al*, 1996). However, only recently has it been demonstrated that the C-terminal domain My13 is involved in myomesin homodimerization, supporting a functional role of the protein in the cross-linking of neighboring myosin filaments across the sarcomeric M-band (Lange *et al*, 2005). The assembly of C-terminal myomesin has been shown to be direct.

We have been able to crystallize a myomesin fragment that comprises the two C-terminal Ig domains My12 and My13. The crystal structure reveals how the myomesin C-terminus is end-to-end assembled and forms a molecular filament of

*Corresponding author. EMBL Hamburg c/o DESY, Notkestrasse 85, Building 25A, Hamburg 22603, Germany.
Tel.: +49 40 89902 110; Fax: +49 40 89902 149;
E-mail: wilmanns@embl-hamburg.de

Received: 9 September 2007; accepted: 6 November 2007; published online: 6 December 2007

14.3 nm in length. The central dimeric interface is formed by β-strand A′ of My13, leading to an intermolecular, antiparallel β-sheet arrangement. In the preceding domain My12, the equivalent β-strand associates with a different β-sheet and is involved in filament propagation rather than assembly. The two Ig domains of each myomesin molecule are connected by a long α-helix, rendering an overall architecture of the assembled myomesin C-terminus that can be associated with three beads-on-the-string model. The overall domain arrangement is different from other known sarcomeric filaments and could become a prototype model for future studies to unravel filament assembly, anchoring and elasticity.

Results

Overall structure of the C-terminal filament assembly of myomesin

We determined the crystal structure of the C-terminal domains My12–My13 (residues 1459–1667) to a resolution of 2.24 Å (Table I, Figure 1). Experimental phases were obtained by the multiple-wavelength anomalous dispersion (MAD) method, using a seleno-methionine-substituted version of the protein. The structure comprises a dimeric assembly of two myomesin molecules, of which all except the five N-terminal residues of the myomesin fragment used for crystallization were interpreted. In addition, 248 ordered solvent molecules were found in the electron density.

The structure reveals an end-to-end dimeric assembly of the two My12–My13 molecules, generating a filament-like shape with overall dimensions of $14.3 \times 5.0 \times 4.1$ nm (Figure 1). The two My13 domains form an extensive antiparallel dimer interface, generating a central two-domain body within the overall architecture. In contrast, the two My12 domains are located at the two tips of the structure. Each of them is connected with the My13 domain of the same molecule by a long α-helix that is partly void of any interactions with the two adjacent My12 and My13 domains. Thus, an overall arrangement of three rigid bodies My12, My13/My13 and My12 is generated, resembling a model of three beads on the string (Figure 1A).

Region variance analysis (Schneider, 2002) confirms this interpretation by identifying two hinges with limited flexibility in symmetric positions, situated at the C-termini of the two My12–My13-connecting helices (Figure 1C). Comparison of relative domain/domain arrangements (Bork *et al*, 1996) reveals an almost identical tilt angle, with a domain rotation along the filament axis of 81° and 82° for the two My12–My13 molecules, respectively. In contrast, the two twist angles, which define the angles of the axes of the two individual Ig domains, are 95° and 124°, revealing a substantial difference of 29° (Figure 1C). Because of these tilt angles, the arrangement of the domains My12 and My13 is far from being linear.

Divergent β-sheet arrangements in domains My12 and My13 support distinct functions

Both the My12 and My13 domains belong to the I-set category of the Ig-fold, which has previously been found in several Ig domains of the protein titin (Marino *et al*, 2005; Zou *et al*, 2006; Muller *et al*, 2007). Apart from local deviations in distinct loop regions, the structures of these domains

Table I X-ray structure determination

Crystal	Native	SeMet substituted		
Data collection				
Space group		$C222_1$		
Cell dimensions *a*, *b*, *c* (Å)	61.50 87.87 203.1	61.58 88.49 203.58		
		Peak	Inflection	Remote
Wavelength	0.8126	0.98214	0.98264	0.91837
Resolution (Å)	20.0–2.24 (2.32–2.24)	15.0–3.06 (3.11–3.06)	15.0–3.06 (3.11–3.06)	15.0–3.20 (3.25–3.20)
R_{merge}[a] (%)	7.6 (38.2)	4.8 (12.8)	5.5 (16.8)	6.6 (14.1)
$\langle I/\sigma I \rangle$	17.8 (3.7)	21.6 (5.4)	17.4 (3.9)	13.9 (4.3)
Completeness (%)	95.7 (93.2)	94.4 (89.8)	94.2 (66.8)	95.8 (77.5)
Redundancy	4.9	2.9	2.7	3.1
Refinement				
Resolution (Å)	20.0–2.24			
No. of reflections	25 014			
R_{cryst}[b]/R_{free}	19.7/22.3			
No. of atoms				
Protein	3489			
Glycerol	24			
Solvent	247			
r.m.s. Δ bonds[c] (Å)	0.012			
r.m.s. Δ angles[c] (deg)	1.380			
Mean *B* factor (Å^2)	44.7			
Main-chain dihedral angles (%)				
Most favored	90.6			
Allowed	9.1			
Generously allowed	0.3			

Parentheses devote values for the highest resolution shell.
[a]$R_{merge} = \sum|I - \langle I \rangle| / \sum I$; *I*, intensity.
[b]$R_{cryst} = \sum|F_o - F_{calc}| / \sum F_o$; F_o, observed structure-factor amplitude; F_{calc}, calculated structure-factor amplitude.
[c]Root-mean-square deviations from ideal values.

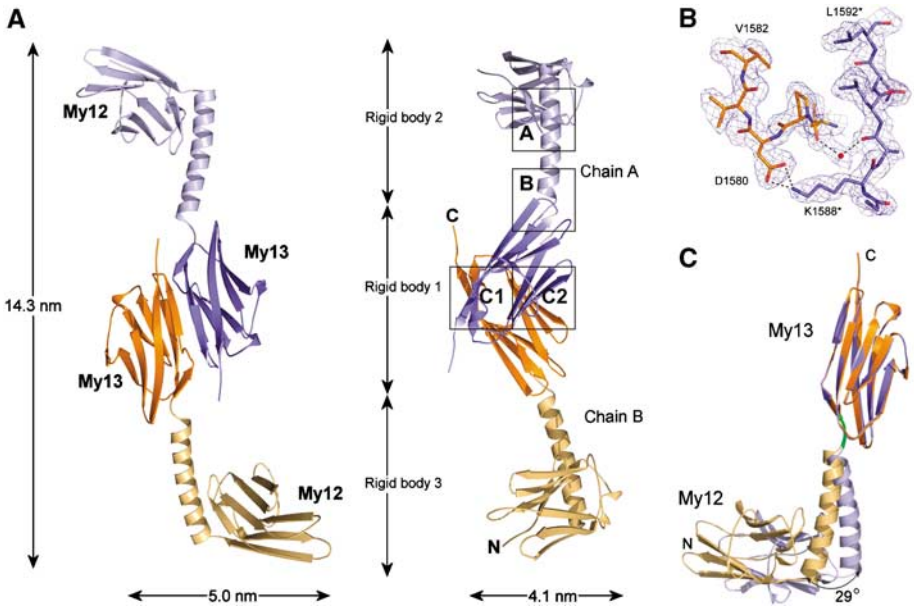

Figure 1 Overall structure of the dimeric filament assembly of the C-terminal myomesin fragment My12–My13. (**A**) Ribbon representation in two different orientations, defining the three rigid body segments: the central $(My13)_2$ assembly and the two distal motifs, each comprising the My12 domain and the My12–My13-connecting α-helix. The two molecules of the dimeric assembly are shown in different colors (orange–light orange/blue–light blue). The dimensions of the overall structure and the three rigid body segments are indicated. Three specific interface regions, including (A) My12/helix , (B) My13/helix and (C1, C2) My13/My13 are framed (right panel). The interfaces are further illustrated in Figures 4 and 5. (**B**) Representative σ_A-weighted $2F_o$–F_c electron density map contoured at 1σ, showing the sequence segments around residues Asp1580 and Lys1588, which form a hydrogen bond in the My13 dimer interface (cp. Figure 5) and which have been used for biochemical validation of the structure (cp. Figure 7). The structure is shown in atom-type colors, following the scheme of panel A for carbon atoms. (**C**) Superposition of the two myomesin molecules, using the coordinates of the My13 domains as common basis. It reveals a 29° difference of the twist angle that determines the relative rotation of My12 and My13 with respect to each other (Bork *et al*, 1996). The hinge is located at the C-terminus of the My12–My13-connecting helix (green).

are generally closely related (Marino *et al*, 2005; Muller *et al*, 2007). However, when the two My12 and My13 Ig domains are superimposed onto each other (Krissinel and Henrick, 2004), their coordinates differ by 1.92 Å (first molecule) and 1.76 Å (second molecule) r.m.s. deviation, thus revealing substantial structural differences (Figure 2). The resulting structure-based alignment comprises only 21% identical amino acids in matching positions (Figure 2A). Direct structural comparison reveals that the N-termini of the two sequences cannot be aligned. Of note, those residues of the My12 domain (1461–1464) that approximately match β-strand A of My13 appear to be in a β-strand-like conformation, but their geometry is too irregular to be recognized as a β-strand. In addition, β-strand G of My13 is four residues longer than that of My12. There are also local conformational differences in loops BC, DE and FG, not allowing a structure-based alignment of the respective sequence segments. Collectively, these structural deviations lead to substantial differences of the overall shapes of the two domains (Figure 3), providing the molecular basis of divergent structural functions of My12 and My13 within the observed end-to-end filament assembly and propagation.

Analysis of the secondary structure topology of the two myomesin Ig domains reveals that β-strand A′ in My12 is associated with a different Ig β-sheet (A′BED) than the equivalent β-strand in My13, which participates in the canonical I-set β-sheet A′GFCC′ (Figure 2B). However, no obvious reason for these structural differences could be discerned, especially considering the similarity in sequence-specific interactions involving residues from β-strand A′ in both domains (not shown). The only noticeable difference in My13 is the interaction between Thr1583 from β-strand A′ and Ser1662 from β-strand G (Figure 2A). In contrast, Ser1470 from My12, which is equivalent to Thr1583 from My13, interacts with one of the main-chain carbonyls of the My12–My13-connecting helix (Figure 4A, right panel). Therefore, the structural swap of strand A′ is most likely caused by the additional interface of the My12 domain with the My12–My13-connecting α-helix (details below). To date, this unusual β-sheet topology has been described only for the growth factor-binding d5 domain of several Trk receptors (Ultsch *et al*, 1999) but has not been found for any sarcomeric protein with long arrays of Ig domains.

The role of the My12–My13-connecting helix in C-terminal myomesin-filament formation

The arrangement of the My12 and My13 Ig domains in the C-terminal myomesin filament is defined by the connecting six-turn α-helix (1549–1570) (Figures 1 and 2B). The helix is amphiphilic over its entire length. The hydrophobic face of its N-terminal part contains an array of aromatic residues (Tyr1551, Tyr1555, Phe1558), followed by one charged residue (Lys1562). The side chains of these residues are at the same face of the helical wheel and provide the framework of an interface with residues from the My12 domain, which is in the order of 540 $Å^2$ (Figure 4A). In particular, Tyr1551 binds into a deep cleft of the My12 domain, which is formed by several residues from the swapped β-strand A′ and the FG loop. The only additional polar interactions, observed in this interface, are two hydrogen bonds, connecting Lys1562 and

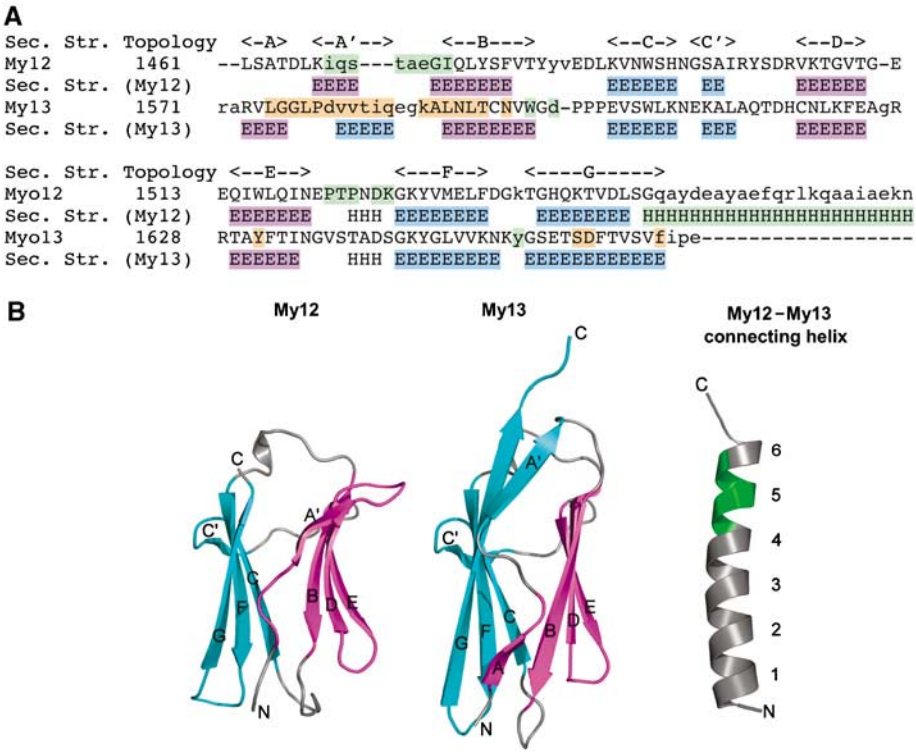

Figure 2 Sequence and structural relations of domains My12 and My13. (**A**) Structure-based sequence alignment. Residue pairs that structurally match are shown in capitals, the remaining ones are in small characters. Those residues that are involved either in interfaces with the My12–My13-connecting α-helix or in the My13 dimer assembly are highlighted in green and orange, respectively. The secondary structural elements are shown below the respective sequences of My12 and My13 (E, β-strand; H, α-helix). The coloring of structural elements indicates association with the first β-sheet (cyan, ABED) and second β-sheet (magenta, A′GFCC′). Please note that β-strand A is missing in My12, and β-strand A′ of My12 has swapped its β-sheet association, taking the canonical I-set arrangement of My13 as reference (Chothia and Jones, 1997). The My12–My13-connecting α-helix is colored in green. The approximate consensus positions of the secondary structural elements, common to My12 and My13, are labeled on top of the alignment. (**B**) Ribbon presentation of the structural modules, My12, My13 and the My12–My13-connecting α-helix. The color codes are as in panel A, except for the My12–My13-connecting helix, in which only the part of the ribbon presenting fully exposed residues is colored in green. The six turns of the helix are numbered.

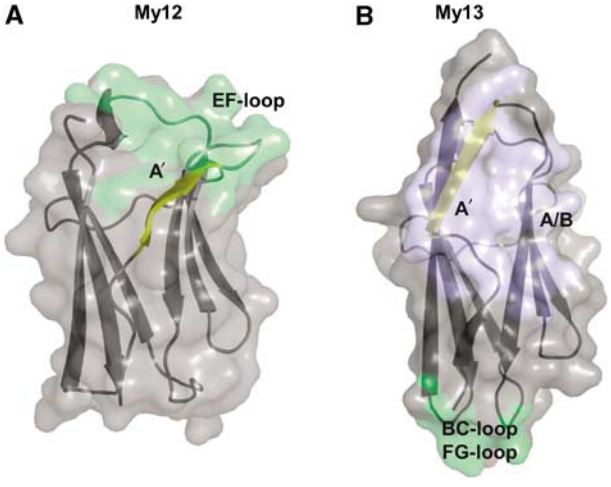

Figure 3 Semitransparent surface presentation of (**A**) My12 and (**B**) My13. The interface areas with the My12–My13-connecting helix and the My13 dimerization interface are colored in green and blue, respectively, demonstrating overlapping interface areas in My12 and My13. The ribbon of each domain is in gray, except β-strand A′ (yellow) that swaps in My12 in terms of β-sheet association. Those structural elements that are involved in interface surfaces are labeled.

Glu1520 from the EF loop, and the main-chain carbonyl group of Ala1554 and the hydroxyl group of Ser1470 from the swapped β-strand A′ of the My12 domain. The interface of the N-terminal part of the helix and the My12 domain is virtually identical in each of the two myomesin molecules, demonstrating a rigid arrangement.

In contrast, the C-terminal part of this connecting α-helix is not involved in lateral interface interactions with any of the two adjacent Ig domains, thus providing an exposed spring-like appearance of this part of the helix. Remarkably, the polar side chains of helix residues Gln1559, Arg1560, Gln1563, Lys1569 and Asn1570 point to the solvent without any interactions to other protein residues. However, an extensive network of capping interactions occurs at the C-terminus of the My12–My13-connecting helix (Figure 4B). Critical contributions are provided by residues Arg1571, Arg1573, Trp1597 and Asn1650 from My13. Arg1573 is the central residue of a negative–positive–negative hydrogen bond network, involving Glu1568 from the C-terminus of the My12–My13-connecting helix. The nature of the My13/helix interface provides a molecular rational for the observed structural deviations in the overall architecture of the myomesin dimer, in contrast to the rigid My12/helix interface (Figure 1C).

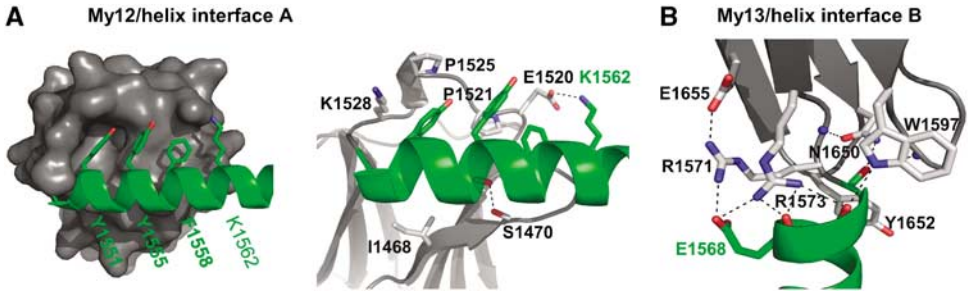

Figure 4 (**A**) My12/helix and (**B**) My13/helix interface. Residues of the My12–My13-connecting α-helix are in green. Those side chains that are involved in one of these interfaces are shown and labeled. Hydrogen bonds are displayed by dashed lines. For the My12/helix interface, a surface presentation (panel A) is also shown to indicate the complementarity of the My12 surface to interact with residues from the N-terminal part of the My12y13-connecting helix. The two interfaces are labeled 'A' and 'B' in Figure 1A.

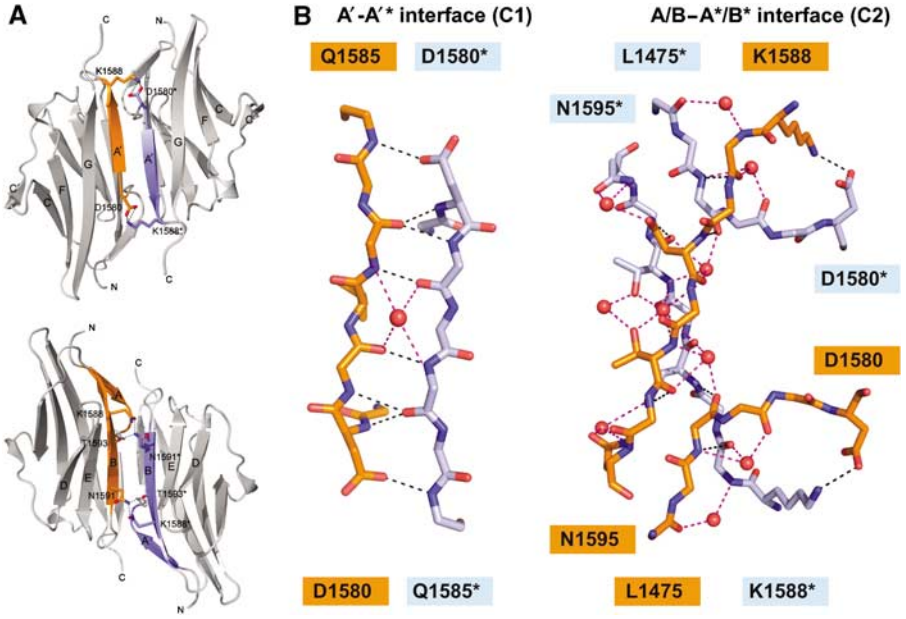

Figure 5 My13 dimerization interface. (**A**) Overview, showing the My13 domain assembly in two different orientations. Upper panel, A′–A′ interface; lower panel, A/B–A/B interface. (**B**) Zoom. Left panel, A′–A′ interface by intermolecular β-sheet interactions of β-strands A′ of the two myomesin molecules; right panel, A/B–A/B interface formed by interactions of several residues from β-strands A and B. The terminal residues of the sequence segments from β-strands A, A′ and B are labeled. Side chains of those residues that are involved in interface interactions are shown. Hydrogen bonds are indicated by dashed lines. Ordered solvent molecules are displayed by red spheres. The color code has been adopted from Figure 1. Labels, referring to the second myomesin molecule of the dimer, are indicated with asterisks. The two interfaces relate to those areas that are labeled C1 and C2 in Figure 1A.

The molecular basis of the end-to-end myomesin-filament assembly

The central dimeric assembly of the C-terminal myomesin filament is defined by a symmetric interface, formed by extensive interactions between the two My13 domains (Figure 5). The interface covers an area of about 710 Å^2 per molecule, corresponding to 12% of the entire My13 surface. It can be basically divided into two parts. The first interaction site is formed by an intermolecular, antiparallel β-sheet with C′CFGA′-A′GFCC′ topology. The regular β-sheet hydrogen-bond pattern extends over residues 1581–1583 from both My13 domains and is symmetrically flanked by a pair of hydrogen bonds, involving the side chain of Asp1580. In addition, one ordered solvent molecule is found in the very center of the intermolecular β-sheet. The second part of the interface is formed by equivalent residues of β-strands A and B from both My13 domains. The β-strands of the second interaction site are, however, not properly oriented to support regular β-sheet interactions. Instead, four symmetrical pairs of separate hydrogen bond pairs are formed: two involving interactions between the C-terminus of β-strand A (Gly1577) and residues from β-strand B (Asn1589, Asn1591); one between residues of β-strand B (Asn1589, Thr1593); and a flanking hydrogen bond by Asp1580 and Lys1588. Moreover, this part of the interface is highly solvated, with a total of 2×5 ordered solvent pairs observed in the X-ray structure. The symmetric arrangement of solvent molecules in this interface is remarkable, considering the limited resolution of the structure and the lack of any non-crystallographic symmetry constraints or restraints imposed upon the structure during structure refinement.

Validation of the molecular architecture of the My12–My13 dimer

Although the described myomesin dimeric assembly is the most prominent within the crystal form used for structure determination, other dimeric assemblies can also be generated in the crystal lattice (Figure 6). To validate the dimeric

arrangement in solution, small-angle X-ray scattering (SAXS) was employed. The scattering pattern computed from the My13-mediated dimer matches the experimental SAXS data with a χ^2 value of 1.58, whereas other potential dimeric assemblies generated from the crystal lattice yielded much poorer fits. Therefore, the SAXS analysis confirms the presence of an end-to-end filament dimer of the myomesin C-terminus that is assembled by the terminal My13 domains.

Further, we mutated two residues (Asp1580 and Lys1588) that form a direct hydrogen bond within the My13 dimerization interface (Figure 5) into residues with opposite charges (Lys1588, Asp1580). As these two residues make critical contributions to the myomesin-dimer interface, we expected that charge reversal of one would diminish or even abolish the entire binding interface. Size exclusion chromatography indeed indicated that both mutants elute with an apparent molecular weight of a monomer (Figure 7A), in contrast to wild-type myomesin. Moreover, SAXS data collected from the two mutants are most compatible with a monomeric association state (Figure 7B and C, Table II). In addition to confirming the crystal structure of My12–My13 dimer, the gel filtration and SAXS data obtained with the mutants reveal that the Asp1580-Lys1588 hydrogen bond within the My13 dimer interface is essential for myomesin homodimerization. The analysis of these mutants also implies that the formation of the antiparallel β-sheet by β-strands A′ from each molecule is not sufficient for constitutive dimer assembly.

In an attempt to test for the dimerization ability of the different combinations of the myomesin C-terminus (wild-type, D1580K, K1588D), we also carried out pull-down experiments using polyhistidine-tagged versions of the three variants (Figure 7D). For all combinations with predicted charge repulsion in the interface (wild-type/D1580K, wild-type/K1588D, D1580K/D1580K, K1588D/K1588D), dimer binding was found to be either largely diminished or completely abolished. Intriguingly, the double mutant D1580K/K1588D was able to partially dimerize, indicating that the dual charge reversal in residues Asp1580 and Lys1588 may allow partial restoration of the My13 dimer interface.

Discussion

Ig-domain-mediated filament assembly and propagation

The architecture of the C-terminal myomesin My12–My13 dimer reveals the molecular basis of a novel type of terminal filament assembly and propagation by a sarcomeric model filament. Our structural findings are consistent with previous yeast two-hybrid interaction and biochemical data, demonstrating direct C-terminal assembly of myomesin via the My13 domain (Lange *et al*, 2005). However, taking into account that more than one-half of a total of 13 myomesin domain modules consist of Ig domains, including two Ig domains (My2, My3) within the N-terminal region and an array of five Ig domains (My9–My13) from the C-terminus of myomesin, the molecular origin of the specific ability of My13 for dimeric assembly remained elusive. Specific My13-mediated myomesin assembly also raises an important question about the underlying molecular parameters of sorting, avoiding unwanted fortuitous assembly with other Ig domains. Moreover, although myomesin-filament cross-linking was considered to be similar to α-actinin links (Lange *et al*, 2005), there have been no data available, to date,

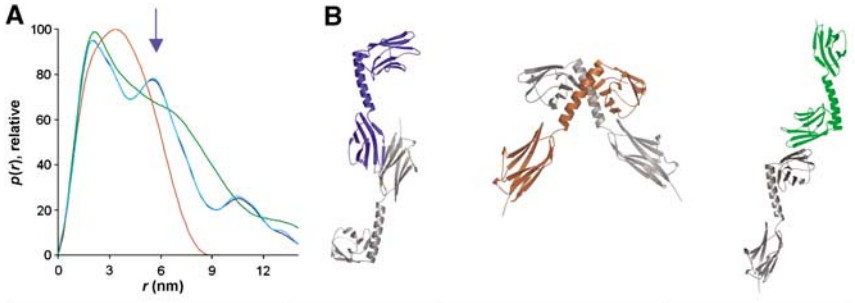

Model	1	2	3
Interface	My13	My12My13 helix	My12
Symmetry operator	*x, y, z*	–x+1/2, y–1/2, –z+1/2	–x+1, y, –z+1/2
Dimer formation (chain)	A/B	A/B	A/A
Interface size (Å^2)	668	815	626
Maximum dimension nm	14.3	8.1	17.5
Radius of gyration nm	3.93	2.90	4.77
Model fit χ^2	1.58	8.0	3.0

Figure 6 SAXS characterization and validation of the dimeric My12–My13 arrangement. (**A**) Distance distribution plots computed for three possible C-terminal myomesin dimer arrangements (model-1, blue; model-2, brown; model-3, green) that can be generated from the crystal lattice. (**B**) Ribbon representations of the three models examined, using the colors of panel A for one molecule of each dimer. The inlet table lists some of the crystallographic model parameters and the agreement with the experimental SAXS data. Comparison with the experimental SAXS curve of *wt*My12–My13 (cp. Figure 7, Table II) demonstrates that the best fit is calculated for model-1, which serves as the basis of structural interpretation. Note that the distance distribution of this model contains an additional maximum at about 6 nm (arrow), reflecting the approximate distance between domains My12 and My13.

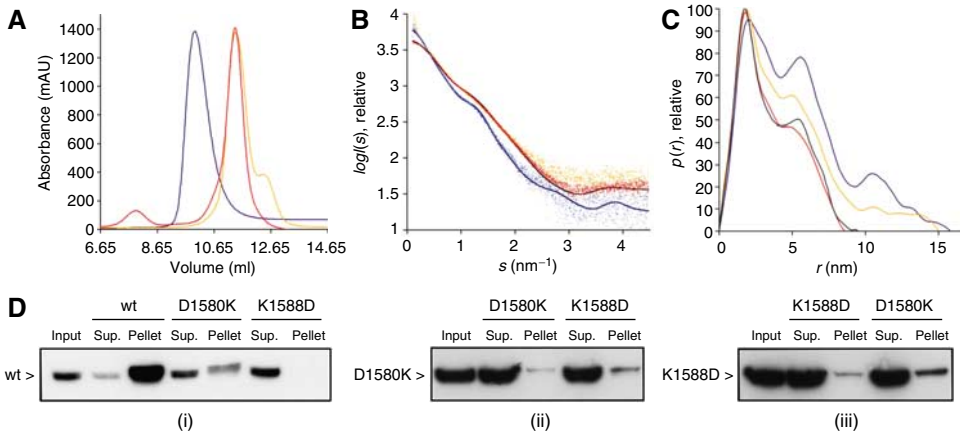

Figure 7 Validation of the My13-mediated dimer interface. (**A**) Size exclusion chromatography of *wt*My12–My13 (blue), My12–My13(D1580K) (orange) and My12–My13(K1588D) (red), indicating that the interaction Asp1580-Lys1588 is essential for dimer formation. (**B**) Experimental SAXS data of *wt*My12–My13 (blue), My12–My13(D1580K) (orange) and My12–My13(K1588D) (red) are shown by data points. They confirm that the interaction D1580-K1588 is essential for dimer formation (cp. Figure 4). The calculated curves of the My12–My13 crystal structure (dimer, blue; one protomer, black) are provided for comparison. (**C**) Distance distributions calculated from the scattering curves in panel B. For one of the mutants (D1580K), the SAXS data, as indicated by the R_g and the $p(r)$ functions, reveal residual dimer formation in the order of 20% (Table II). (**D**) Pull-down assays, using (i) wtMy12–My13, (ii) My12–My13(D1580K), (iii) My12–My13(K1588D), indicating that charge reversal of either Asp1580 or Lys1588 impairs My12–My13 dimer formation. In contrast, charge reversal in both residues selected for site-directed mutagenesis (D1580K, K1588D) partially restores the ability of myomesin to dimerize.

Table II SAXS data collection statistics of the myomesin My12My13 fragment and its mutants D1580K and K1588D

Sample	My1213	My1213 D1580K	My1213 K1588D
Theoretical molecular mass (kDa)[a]	23.4	23.4	23.4
Experimental molecular mass (kDa)[b]	47±4	21±2	20±2
Maximum size, d_{max} X-ray model (nm)[c]	14.1	10.0	10.0
Experimental maximum size, d_{max} Gnom (nm)[d]	14±1.5	13±1.5	9±1
Radius of gyration, R_g X-ray model (nm)[d]	3.93	2.79	2.79
Experimental radius of gyration R_g (nm)[d]	4.04±0.08	3.30±0.05	2.77±0.05
Model fit, χ against raw data (monomer)	5.4	1.16	0.90
Model fit, χ against raw data (dimer)	1.58	2.80	8.6
Monomer/dimmer fraction (%)[e]	7/93	78/22	100/0

[a]Molecular mass of the monomeric construct calculated from the sequence.
[b]Molecular mass from comparison with reference solutions of BSA.
[c]For the D1580K, K1588D mutants: calculations against chain A of the crystallographic model.
[d]Maximum particle dimension and radius of gyration calculated by indirect transformation of the scattering data using GNOM.
[e]The volume fractions are calculated by the best fits of the experimental data by the curves computed from monomeric and dimeric constructs. The accuracy of the estimate is about 5%.

providing a molecular model of myomesin-filament propagation from the C-terminal assembly.

The crystal structure of the C-terminal myomesin dimer reveals how two domains that both belong to the same I-set Ig domain category perform different functions within the context of a large structural protein, leading to filament assembly (My13) and propagation (My12). To detect specific structural differences within the two Ig domains My12 and My13, we made use of previously defined structural markers of this fold (Chothia and Jones, 1997). One of the specific features of the I-set family of Ig domains is the presence of an additional β-strand A′. In the canonical I-set arrangement, this strand interacts with the second β-sheet of A′GFC topology, whereas the preceding β-strand A associates with the first Ig domain β-sheet of ABED topology.

Structural comparison of the My12 and My13 Ig domains has identified the N-terminal sequence segment as the most divergent region (Figure 2). The difference is highlighted by an unexpected swapped association of β-strand A′ in the myomesin My12 domain, using the My13 arrangement and other canonical I-set Ig domains from titin (Marino *et al*, 2005; Muller *et al*, 2007) as reference. The different β-sheet association of this strand in domains My12 and My13 leads to distinct structural functions of residues from β-strand A′. Whereas in My12 the strand is critically involved in the formation of an intramolecular interface with the My12–My13-connecting α-helix, in My13 the same strand forms an intermolecular antiparallel β-sheet arrangement over six residues with the equivalent strand of the second myomesin My13 domain (Figures 4 and 5B).

However, as this My13/My13 β-sheet is formed by main-chain atom interactions, this type of interface on its own may not be sufficient to avoid fortuitous β-sheet assembly with other I-set Ig domains from myomesin- or different sarcomeric-filament proteins. The structure of the My12–My13 dimer and biochemical validation data demonstrate that additional sequence-specific interactions, originating from residues on β-strands A and B, are essential for the formation

of the My13 dimerization interface (Figure 4B). For instance, abolishment of the charged hydrogen bond by Asp1580 and Lys1588 impairs My13-mediated terminal myomesin dimer assembly (Figure 7).

In contrast, the swapped β-sheet association of β-strand A′ in My12 does not support the formation of a My13-like dimer interface by the My12 domain. Thus, our present data demonstrate how specific structural rearrangements in domains with an identical fold can lead to different functional readouts, either My13-mediated myomesin-filament assembly or the formation of a specific helix interface by My12 that provides the structural basis of filament propagation within the My12–My13 dimer. Moreover, comparison of the sequences of My12 and further preceding Ig domains from myomesin (My9, My10, My11) does not reveal any conservation of residues involved in the My13 dimer interface (data not shown), thus making it unlikely that any of these domains may have the ability to form a My13-like dimer interface.

The My12–My13 structure displays the propagation of single myomesin filaments, originating from the C-terminal My13 end-to-end assembly. Our data are in agreement with previous *in vivo* and biochemical data that point to the presence of single myomesin-filament strands rather than oligomeric rod assemblies (Obermann *et al*, 1996; Lange *et al*, 2005). In contrast, even though Ig domain-mediated terminal assemblies have been demonstrated in filamentous proteins like titin and different filamin isoforms (McCoy *et al*, 1999; Popowicz *et al*, 2004; Pudas *et al*, 2005; Zou *et al*, 2006), it is unlikely or unknown whether the antiparallel arrangement of the assembly site propagates throughout the remaining filament of these proteins. Based on structural data of human filamin C, a flexible hinge region near the dimerization module was proposed (Pudas *et al*, 2005). This model attempted to reconcile the observed antiparallel assembly of the C-terminal domain observed in the crystal structure with previous electron microscopy data that supported a parallel rod arrangement. However, in the C-terminal myomesin filament, the structural rigidity of the Ig domain-connecting α-helical linker does not allow comparable bending, which could lead to a reversal of the overall filament orientation. The concept of single-filament propagation for myomesin is also unrelated to the type of filament formation in α-actinin, which is oligomeric and formed by α-helical coiled coil domains instead of Ig domains (Djinovic-Carugo *et al*, 1999). Interestingly, the individual domains of the α-actinin rod R1–R4 are also connected by α-helical linkers, which are, however, short and not exposed to the external solvent over several residues.

Does the My12–My13-connecting helix function as an elastic spring?

Intensive research on the molecular parameters leading to passive elasticity of the giant muscle protein titin has revealed that the flexible 'PEVK' regions within the I-band segment give rise to most of the protein's elastic properties, whereas the involvement of folded Ig or Fn domains remains controversial (Preetha *et al*, 2005; Tskhovrebova *et al*, 2005). Similar to titin, a recent model also postulated a molecular requirement for elastic properties in myomesin, to build flexible bridges to the titin and myosin filaments under substantial external force conditions *in vivo* (Agarkova and Perriard, 2005). Recent data, using single-molecule force spectroscopy and transmission electron microscopy, demonstrated that the embryonic heart (EH) segment within the central part of the EH isoform of myomesin may act as an entropic spring (Bertoncini *et al*, 2005; Schoenauer *et al*, 2005). However, the entire C-terminal Ig domain array My9–My13 of myomesin, in the absence of high-resolution structural data, has not been investigated in terms of potential elastic properties of the protein, to date.

Nonetheless, the structure of the dimeric My12–My13 filament provides an unexpected model to test molecular elasticity of the C-terminal part of myomesin. In contrast to other known Ig domain arrays with available 3D structures (Zou *et al*, 2006; Mrosek *et al*, 2007; Muller *et al*, 2007), domains My12 and My13 of myomesin are linked by an α-helix, of which about one-half is void of any interactions with other protein residues of the myomesin C-terminus (Figure 8). This finding is remarkable, considering that fully exposed α-helices are not commonly found as domain connecting elements in soluble proteins. Indeed, they are like a mechanical coiled spring, universally used in natural processes requiring elasticity (Chouaieb *et al*, 2006).

In contrast to amphiphilic or hydrophobic helices, which are generally either embedded in sidewise interactions with other protein residues or assembled into coiled coils, the mechanical stability of a structurally separate helix, like that observed for the C-terminal part of the My12–My13-connecting helix, is solely determined by the internal α-helical hydrogen-bond pattern. Previous measurements revealed that only low mechanical forces below 30 pN are required to disrupt the internal hydrogen-bond pattern (Choe and Sun, 2005; Root *et al*, 2006). Previous experimental and computational data investigating the mechanical stability of the cytoskeletal protein spectrin are consistent with our hypotheses, as they demonstrate a distinct and reversible stretching-out pattern of α-helical linker regions under low external force conditions (Rief *et al*, 1999; Law *et al*, 2003). Considering the exposure of myomesin to external forces within sarcomeres (Agarkova and Perriard, 2005), the mechanical stability of such helical linker may be inferior to that of domain/domain arrangements investigated previously or comparable to the measured elastic properties of the EH region (Bertoncini *et al*, 2005; Schoenauer *et al*, 2005). Similar investigations for the C-terminal myomesin filament, taking advantage of the structural knowledge of the domain/domain linkers in My12–My13, are eagerly awaited. However, such studies will require an extension of the present analysis of the C-terminal My12–My13 fragment into a larger array of C-terminal myomesin Ig domains.

My12–My13 as model for a repetitive filament architecture in myomesin

Using a suite of secondary structure prediction programs (Rost *et al*, 2004), the length and the position of the My12–My13-connecting helix can be accurately predicted with high confidence values (Figure 8C). Extending our analysis over the entire C-terminal half of the myomesin sequence, spanning five Ig domains (My9–My13), we predict a repetitive pattern of α-helices at basically identical sequence intervals of about 110 residues (Figure 8C), also with high confidence values. The predicted helices are consistently located in sequence segments between myomesin Ig domains My9–

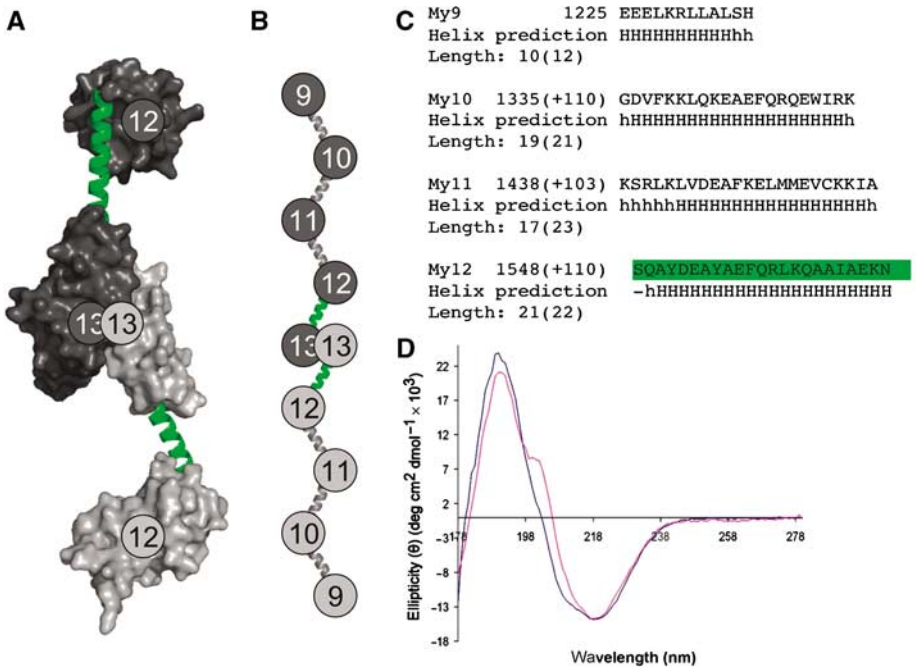

Figure 8 Prediction of a myomesin filament beads-on-the-string model, consisting of 2 × 5 Ig domains that are connected by α-helical linkers and end-to-end C-terminal assembly. (**A**) Beads-on-the-string presentation of the crystal structure of the My12–My13 dimeric assembly of the myomesin C-terminus (cp. Figure 1). (**B**) Schematic model of the My9–My13 C-terminal filament, in which adjacent domains are connected by α-helical linkers. (**C**) Prediction of α-helical segments at repetitive sequence intervals, interspersed myomesin domains My9, My10, My11, My12 and My13, using PredictProtein (Rost *et al*, 2004). The starting residue number, the sequence interval with respect to the previous predicted α-helical segment and the sequence of each predicted α-helix segment are presented. Residues that are predicted to be α-helical by PROF (for details, see PredictProtein) are shown in capital characters, and those that are predicted with a confidence level of at least 82% are shown by small characters. The predicted helix length, using the two categories, is indicated (second number in parentheses). For comparison, the experimentally determined My12–My13-connecting helix is highlighted in green. (**D**) Circular dichroism curves of My12–My13 (blue) and My9–My13 (magenta). The estimates for secondary structural elements for My12–My13 and My9–My13 are as follows: helix, 0.23/0.19; strand, 0.26/0.36; turn, 0.18/0.13; unordered, 0.33/0.34.

My13. The prediction is supported by circular dichroism spectra of the myomesin fragments My12–My13 and My9–My13 (Figure 8D). Both constructs show a significant α-helical content of about 20%. We are not aware about a similar pattern reported for any other sarcomeric protein.

Thus, the above findings support the emergence of an attractive filament model of a repetitive array of Ig domain/linker repeats, which may form the molecular basis of the filament architecture of myomesin over long distances (Obermann *et al*, 1996; Lange *et al*, 2005). Previous immunoelectron microscopy data found that the N-terminal part of myomesin is located at or close to the symmetric M4 and M4′ lines of the sarcomeric M band, whereas domains of the C-terminal Ig domain array of myomesin are located between the two lines (Obermann *et al*, 1996). Recent biochemical data (Lange *et al*, 2005) and our present data, demonstrating C-terminal dimeric assembly of myomesin, therefore suggest that the C-terminal half of myomesin, spanning domains My9–My13, functions as a bridging filament. Such filament would allow to connect protein components with myomesin interaction sites that have been found in the M4/M4′ lines, such as creatine kinase (Hornemann *et al*, 2003) and titin (Obermann *et al*, 1997), across the central M line through the C-terminal myomesin filament.

A repetitive domain structure for My9–My13 is expected to lead to a dimeric myomesin end-to-end filament with a total of 4 × 2 Ig-domain/helix modules (My9, My10, My11, My12) and one central My13 dimerization unit. If we estimate each domain module to be in the order of 6 nm in length, using the My12–My13 crystal structure and the SAXS distribution function as reference (Figures 1 and 7C), such myomesin My9–My13 filament would be about 55 nm long, assuming a fully extended arrangement of adjacent domains. However, as our structural data indicate a filament with twist angles that would considerably deviate from a linear arrangement (Figure 1), such a filament may approach the estimated M4/M4′ distance of 44 nm in the relaxed sarcomere state.

At present, the lack of available experimental data of the C-terminal myomesin Ig-domain array beyond the My12–My13 fragment prevents further speculations. To confirm the molecular filament architecture of the entire C-terminal Ig array of myomesin, therefore, a combination of high-resolution structural biology methods and solution methods, allowing molecular imaging *in vitro* and *in vivo*, will be required. Should the presence of an array of repetitive Ig-domain helix linker elements be experimentally confirmed, the C-terminal myomesin filament could become a unique model system to study molecular mechanisms of protein elasticity mediated by long-distance filament cross-linkers under physiological conditions.

Materials and methods

Protein expression and purification

The DNA sequence (Q6H969_HUMAN) encoding for myomesin domains My12–My13 (residues 1459–1667) was amplified by PCR from existing constructs (Lange *et al*, 2005), using primers to generate XhoI and MluI sites at the 5′ and 3′ ends, respectively. The DNA fragments were digested and inserted into a

modified pET22b(+) vector (Novagen) carrying an N-terminal polyhistidine-tag sequence and a TEV protease cleavage site. The My12–My13 fragment and the versions of its two single-point mutants D1580K and K1588D were overexpressed in the *Escherichia coli* strain BL21(DE3) and induced with 1 mM IPTG. For production of the seleno-L-methionine (SeMet)-incorporated My12–My13-domain construct, the corresponding expression vector was used to transform the methionine auxotroph *E. coli* strain B834(DE3). A preculture grown in LB broth medium was washed with M9 minimal medium and resuspended in 1.5 l of medium A (M9 supplied with 20 mM D-(+)-glucose, 1 mM $MgCl_2$, 0.3 mM $CaCl_2$, 4 μM biotin, 2.7 μM thiamine) and trace element solution (0.3 mM $FeCl_3 \cdot 6H_2O$, 0.06 mM $ZnCl_2$, 0.008 mM $CuCl_2 \cdot 4H_2O$, 0.004 mM $CoCl_2 \cdot 6H_2O$, 0.016 mM H_3BO_3, 0.0007 mM $MnCl_2 \cdot 6H_2O$). The cells were grown at 310 K for 3 h (starvation step) before adding the L-amino acids mixture (40 μg ml^{-1} of each amino acid, except methionine) and SeMet (60 μg ml^{-1}). When the culture entered the logarithmic phase of growth, it was induced with 1 mM IPTG and grown overnight. All proteins were purified from crude cell extracts using Ni-NTA affinity chromatography, followed by removal of the hexahistidine tag by TEV protease. The proteins were further purified by size-exclusion chromatography, using a Superdex 200 column (16/60 or 10/30), equilibrated with 25 mM Tris/HCl, pH 7.5, and 150 mM NaCl. The wild type and SeMet version of My12–My13 eluted with an apparent molecular weight of approximately 48 kDa, matching the molecular weight of a dimer, whereas the single-point mutants were eluted as monomers.

X-ray structure determination and interpretation

The myomesin My12–My13 fragment was crystallized by the hanging-drop vapor diffusion technique. Of about 10 mg ml^{-1} of protein solution, 1 μl was mixed with 1 μl of 14% (w/v) PEG 20000, 0.1 M, Bis-Tris, pH 7.5, and 0.16 M ammonium acetate and suspended above a reservoir of the same solution. Crystals of a trigonal shape appeared the next day and grew to an optimal size of about $200 \times 200 \times 50\,\mu m^3$ within one week. They were identified to belong to space group $C222_1$, containing two copies of the molecule per asymmetric unit, with a solvent content of 56.5% (Matthews, 1968).

A MAD experiment using the SeMet protein was carried out on the tunable wiggler beamline BW7A (EMBL/DESY, Hamburg, Germany) and a native data set was collected on the bending magnet beamline X11 (EMBL/DESY, Hamburg, Germany). Before data collection, the crystals were immersed in the mother liquid containing 18% (v/v) MPD and flash cooled at 100K under the cryostream attached to the goniometer. All data sets were integrated, scaled and merged using the HKL suite (Otwinowski and Minor, 1997). The expected two selenium atoms were located using the heavy-atom search routine of the CNS program suite (Brunger *et al*, 1998). These positions were refined; initial phases of the protein were calculated to 3.1 Å resolution, and density modification was applied, improving the figure of merit from 0.455 to 0.898 as defined in CNS (Brunger *et al*, 1998). The electron density map was of sufficient quality to fit the titin module M5 NMR model (PDB code: 1NCT) by phased molecular replacement (Murshudov *et al*, 1997) at the two positions of the domain My13. The remaining model was built manually using the program 'O' (Jones *et al*, 1991). Further refinement using molecular dynamics (CNS) resulted in a map where the entire protein model, except for the first five disordered residues, could be built. Solvent molecules were added by ARP/wARP (Perrakis *et al*, 2001), and the final cycles of refinement were carried out through REFMAC5, using TLS refinement of rigid groups (Winn *et al*, 2001). The data collection and refinement statistics are reported in Table I.

A structure-based sequence alignment was computed by SSM (Krissinel and Henrick, 2004). Protein/protein interfaces were determined with the program AREAIMOL of the CCP4 suite (Collaborative Computational Project, 1994). Secondary structural elements were determined by PROCHECK (Laskowski *et al*, 1993).

SAXS analysis

Measurements were carried out at the beamline X33 (EMBL/DESY, Hamburg, Germany). Each sample was exposed to X-rays of wavelength $\lambda = 1.5$ Å for 3 min, and the signal was recorded on a MAR345 IP detector. The measurements were carried out at 290 K using a sample-detector distance of 2.7 m, with a momentum transfer range of $0.10\,nm^{-1} < s < 4.5\,nm^{-1}$ (here, $s = 4\pi \sin(\theta)/\lambda$ where 2θ is the scattering angle). All myomesin samples were measured at, at least, two different concentrations with intermittent buffer solution (25 mM Tris/HCl, pH 7.5, and 150 mM NaCl). To monitor radiation damage, two consecutive 2 min exposures at the highest protein concentration were compared. The data were processed using standard procedures, corrected for buffer contribution and extrapolated to infinite dilution using the program PRIMUS (Konarev *et al*, 2003). The radius of gyration R_g and forward scattering $I(0)$, the maximum particle dimension D_{max} and the distance distribution function $p(r)$ were evaluated using the program GNOM (Svergun, 1992). The molecular masses of the different constructs were calculated by comparing with the reference bovine serum albumin (BSA) samples. The scattering patterns from the high-resolution models were calculated using the program CRYSOL (Svergun *et al*, 1995). The best fits in terms of mixtures of monomers and dimers for My12–My13 mutants were computed using the program OLIGOMER (Konarev *et al*, 2003).

The discrepancy of the experimental data was calculated as follows:

$$\chi^2 = \frac{1}{N-1} \sum_j \left[\frac{I_{exp}(s_j) - cI_{calc}(s_j)}{\sigma(s_j)} \right]^2,$$

where N is the number of experimental points, c is a scaling factor and $I_{calc}(s)$ and $\sigma(s_j)$ are the calculated intensity and the experimental error at the momentum transfer s_j, respectively. The SAXS data statistics are summarized in Table II.

Circular dichroism measurements

The myomesin fragments My12–My13 and My9–My13 were dialyzed against 30 mM potassium phosphate, pH 7.5. The concentration of each sample was determined by measuring the absorbance of the proteins, which were diluted with 8 M urea. Far-UV circular dichroism (CD) spectra were obtained on station 12.1 at the Synchrotron Radiation Source (Daresbury Laboratory, UK). Experiments were performed at a temperature of 277 K and a wavelength range of 280–175 nm. The spectra were analyzed with the CONTIN procedure (Provencher and Glockner, 1981).

Biochemical characterization

GFP-labeled myomesin My9–My13 constructs (residues 1134–1685) were generated via PCR and subcloned into the pEGFP-C1 vector (Clontech). Site-directed mutagenesis to produce the D1580K and the K1588D mutants was carried out as per the Quickchange protocol (Stratagene). All constructs and mutants were verified by sequencing. For the pull-down assay, Cos-1 cells were transfected with the GFP constructs using Escort IV (Sigma), and expression was measured after 2 days. Cells were lysed in IP-buffer (150 mM NaCl, 10 mM Tris-HCl, pH 7.9, 1 mM DTT, 0.2% NP-40, 1 × Roche Protease Inhibitor Cocktail), sonicated briefly and centrifuged at 4°C to separate the soluble and insoluble cell fractions. The soluble Cos-lysate fraction was incubated with His-tagged My12–My13 (wild type), My12–My13 (D1580K), or My12–My13 (K1588D) bound to Ni-NTA beads (Qiagen) for 2 h on ice. Beads were washed three times with ice-cold IP buffer and samples were processed for SDS–PAGE followed by immunoblotting. Visualization of GFP-tagged proteins was done using the monoclonal mouse anti-GFP antibody (Roche) followed by a horseradish peroxidase-coupled rabbit anti-mouse antibody (DAKO).

Accession numbers

The coordinates and the structure factors were deposited in the Protein Data Bank with accession code 2R15.

Acknowledgements

We thank PV Konarev for supporting the SAXS experiments at beamline X33 (EMBL/DESY, Hamburg, Germany), DT Clarke and A Brown for supporting the CD experiments at beamline CD12 (Daresbury) as well as the CCLRC Daresbury Laboratory's Synchrotron Radiation Source for financial support. NP and SL were supported by the EU research and training network CAMKIN (HPRN-CT-2002-00252) to MW and Professor Mathias Gautel, respectively. The project was also supported by a grant of the FWF (P19060-B12). We thank Mathias Gautel, Elisabeth Ehler and Irina Agarkova for critical suggestions and fruitful discussions.

References

Agarkova I, Perriard JC (2005) The M-band: an elastic web that crosslinks thick filaments in the center of the sarcomere. *Trends Cell Biol* **15:** 477–485

Bertoncini P, Schoenauer R, Agarkova I, Hegner M, Perriard JC, Guntherodt HJ (2005) Study of the mechanical properties of myomesin proteins using dynamic force spectroscopy. *J Mol Biol* **348:** 1127–1137

Bork P, Downing AK, Kieffer B, Campbell ID (1996) Structure and distribution of modules in extracellular proteins. *Q Rev Biophys* **29:** 119–167

Brunger AT, Adams PD, Clore GM, DeLano WL, Gros P, Grosse-Kunstleve RW, Jiang JS, Kuszewski J, Nilges M, Pannu NS, Read RJ, Rice LM, Simonson T, Warren GL (1998) Crystallography & NMR system: a new software suite for macromolecular structure determination. *Acta Crystallogr D Biol Crystallogr* **54:** 905–921

Choe S, Sun SX (2005) The elasticity of alpha-helices. *J Chem Phys* **122:** 244912

Chothia C, Jones EY (1997) The molecular structure of cell adhesion molecules. *Annu Rev Biochem* **66:** 823–862

Chouaieb N, Goriely A, Maddocks JH (2006) Helices. *Proc Natl Acad Sci USA* **103:** 9398–9403

Collaborative Computational Project, Number 4 (1994) The CCP4 suite: programs for protein crystallography. *Acta Crystallogr D Biol Crystallogr* **D50:** 760–763

Djinovic-Carugo K, Young P, Gautel M, Saraste M (1999) Structure of the alpha-actinin rod: molecular basis for cross-linking of actin filaments. *Cell* **98:** 537–546

Hornemann T, Kempa S, Himmel M, Hayess K, Furst DO, Wallimann T (2003) Muscle-type creatine kinase interacts with central domains of the M-band proteins myomesin and M-protein. *J Mol Biol* **332:** 877–887

Jones TA, Zou JY, Cowan SW, Kjeldgaard M (1991) Improved methods for binding protein models in electron density maps and the location of errors in these models. *Acta Crystallogr A* **47:** 110–119

Kenny PA, Liston EM, Higgins DG (1999) Molecular evolution of immunoglobulin and fibronectin domains in titin and related muscle proteins. *Gene* **232:** 11–23

Konarev PV, Volkov VV, Sokolova AV, Koch MHJ, Svergun DI (2003) PRIMUS: a windows PC-based system for small-angle scattering data analysis. *J Appl Cryst* **36:** 1277–1282

Krissinel E, Henrick K (2004) Secondary-structure matching (SSM), a new tool for fast protein structure alignment in three dimensions. *Acta Crystallogr D Biol Crystallogr* **60:** 2256–2268

Labeit S, Kolmerer B, Linke WA (1997) The giant protein titin. Emerging roles in physiology and pathophysiology. *Circ Res* **80:** 290–294

Lange S, Ehler E, Gautel M (2006) From A to Z and back? Multicompartment proteins in the sarcomere. *Trends Cell Biol* **16:** 11–18

Lange S, Himmel M, Auerbach D, Agarkova I, Hayess K, Furst DO, Perriard JC, Ehler E (2005) Dimerisation of myomesin: implications for the structure of the sarcomeric M-band. *J Mol Biol* **345:** 289–298

Laskowski RA, MacArthur MW, Moss DS, Thornton JM (1993) PROCHECK: a program to check the stereochemical quality of protein structures. *J Appl Cryst* **26:** 283–291

Law R, Carl P, Harper S, Dalhaimer P, Speicher DW, Discher DE (2003) Cooperativity in forced unfolding of tandem spectrin repeats. *Biophys J* **84:** 533–544

Li H, Linke WA, Oberhauser AF, Carrion-Vazquez M, Kerkvliet JG, Lu H, Marszalek PE, Fernandez JM (2002) Reverse engineering of the giant muscle protein titin. *Nature* **418:** 998–1002

Marino M, Svergun DI, Kreplak L, Konarev PV, Maco B, Labeit D, Mayans O (2005) Poly-Ig tandems from I-band titin share extended domain arrangements irrespective of the distinct features of their modular constituents. *J Muscle Res Cell Motil* **26:** 355–365

Matthews BW (1968) Solvent content of protein crystals. *J Mol Biol* **33:** 491–497

McCoy AJ, Fucini P, Noegel AA, Stewart M (1999) Structural basis for dimerization of the Dictyostelium gelation factor (ABP120) rod. *Nat Struct Biol* **6:** 836–841

Mrosek M, Labeit D, Witt S, Heerklotz H, von Castelmur E, Labeit S, Mayans O (2007) Molecular determinants for the recruitment of the ubiquitin-ligase MuRF-1 onto M-line titin. *FASEB J* **21:** 1383–1392

Muller S, Lange S, Gautel M, Wilmanns M (2007) Rigid conformation of an immunoglobulin domain tandem repeat in the A-band of the elastic muscle protein titin. *J Mol Biol* **371:** 469–480

Murshudov GN, Vagin AA, Dodson EJ (1997) Refinement of macromolecular structures by the maximum-likelihood method. *Acta Crystallogr D Biol Crystallogr* **53:** 240–255

Obermann WM, Gautel M, Steiner F, van der Ven PF, Weber K, Furst DO (1996) The structure of the sarcomeric M band: localization of defined domains of myomesin, M-protein, and the 250-kD carboxy-terminal region of titin by immunoelectron microscopy. *J Cell Biol* **134:** 1441–1453

Obermann WM, Gautel M, Weber K, Furst DO (1997) Molecular structure of the sarcomeric M band: mapping of titin and myosin binding domains in myomesin and the identification of a potential regulatory phosphorylation site in myomesin. *EMBO J* **16:** 211–220

Otwinowski Z, Minor V (1997) Processing of X-ray diffraction data collected in oscillation mode. *Methods Enzymol* **276:** 307–326

Perrakis A, Harkiolaki M, Wilson KS, Lamzin VS (2001) ARP/wARP and molecular replacement. *Acta Crystallogr D Biol Crystallogr* **57:** 1445–1450

Popowicz GM, Muller R, Noegel AA, Schleicher M, Huber R, Holak TA (2004) Molecular structure of the rod domain of dictyostelium filamin. *J Mol Biol* **342:** 1637–1646

Preetha N, Yiming W, Helmes M, Norio F, Siegfried L, Granzier H (2005) Restoring force development by titin/connectin and assessment of Ig domain unfolding. *J Muscle Res Cell Motil* **26:** 307–317

Provencher SW, Glockner J (1981) Estimation of globular protein secondary structure from circular dichroism. *Biochemistry* **20:** 33–37

Pudas R, Kiema TR, Butler PJ, Stewart M, Ylanne J (2005) Structural basis for vertebrate filamin dimerization. *Structure* **13:** 111–119

Rief M, Pascual J, Saraste M, Gaub HE (1999) Single molecule force spectroscopy of spectrin repeats: low unfolding forces in helix bundles. *J Mol Biol* **286:** 553–561

Root DD, Yadavalli VK, Forbes JG, Wang K (2006) Coiled-coil nanomechanics and uncoiling and unfolding of the superhelix and alpha-helices of myosin. *Biophys J* **90:** 2852–2866

Rost B, Yachdav G, Liu J (2004) The PredictProtein server. *Nucleic Acids Res* **32:** W321–W326

Schneider TR (2002) A genetic algorithm for the identification of conformationally invariant regions in protein molecules. *Acta Crystallogr D Biol Crystallogr* **58:** 195–208

Schoenauer R, Bertoncini P, Machaidze G, Aebi U, Perriard JC, Hegner M, Agarkova I (2005) Myomesin is a molecular spring with adaptable elasticity. *J Mol Biol* **349:** 367–379

Sotomayor M, Schulten K (2007) Single-molecule experiments *in vitro* and *in silico*. *Science* **316:** 1144–1148

Svergun D, Barberato C, Koch MHJ (1995) CRYSOL—a program to evaluate X-ray solution scattering of biological macromolecules from atomic coordinates. *J Appl Cryst* **28:** 768–773

Svergun DI (1992) Determination of the regularization parameter in indirect-transform methods using perceptual criteria. *J Appl Cryst* **25:** 495–503

Tskhovrebova L, Trinick J (2003) Titin: properties and family relationships. *Nat Rev Mol Cell Biol* **4:** 679–689

Tskhovrebova L, Houmeida A, Trinick J (2005) Can the passive elasticity of muscle be explained directly from the mechanics of individual titin molecules? *J Muscle Res Cell Motil* **26:** 285–289

Ultsch MH, Wiesmann C, Simmons LC, Henrich J, Yang M, Reilly D, Bass SH, de Vos AM (1999) Crystal structures of the neurotrophin-binding domain of TrkA, TrkB and TrkC. *J Mol Biol* **290:** 149–159

Vinkemeier U, Obermann W, Weber K, Furst DO (1993) The globular head domain of titin extends into the center of the sarcomeric M band. cDNA cloning, epitope mapping and immunoelectron microscopy of two titin-associated proteins. *J Cell Sci* **106** (Part 1)**:** 319–330

Watanabe K, Muhle-Goll C, Kellermayer MS, Labeit S, Granzier H (2002) Different molecular mechanics displayed by titin's

constitutively and differentially expressed tandem Ig segments. *J Struct Biol* **137:** 248–258

Weinert S, Bergmann N, Luo X, Erdmann B, Gotthardt M (2006) M line-deficient titin causes cardiac lethality through impaired maturation of the sarcomere. *J Cell Biol* **173:** 559–570

Williams PM, Fowler SB, Best RB, Toca-Herrera JL, Scott KA, Steward A, Clarke J (2003) Hidden complexity in the mechanical properties of titin. *Nature* **422:** 446–449

Winn MD, Isupov MN, Murshudov GN (2001) Use of TLS parameters to model anisotropic displacements in macromolecular refinement. *Acta Crystallogr D Biol Crystallogr* **57:** 122–133

Zou P, Pinotsis N, Lange S, Song YH, Popov A, Mavridis I, Mayans OM, Gautel M, Wilmanns M (2006) Palindromic assembly of the giant muscle protein titin in the sarcomeric Z-disk. *Nature* **439:** 229–233